Paper 11B.3: **The need for caution when interpreting velocity field structures predicted by LES** by F. Ludwig, F. Chow, & R. Street
Amer. Meteorol. Soc., 18th Symp. on Boundary Layers & Turbulence, June 2008, Stockholm, Sweden

The need for caution when interpreting velocity field structures predicted by LES

Francis L. Ludwig[1], Stanford University, Stanford, CA
Fotini Katopodes Chow, University of California, Berkeley, CA
Robert L. Street, Stanford University, Stanford, CA

1. Introduction

Large eddy simulation (LES) is often used to study atmospheric behavior on scales of hundreds of meters, because off-the-shelf LES models that represent small scales as bulk effects at resolved scales can be run at reasonable cost. This ease of use compared with laboratory or field experiments has led to many numerical studies of atmospheric boundary layer behavior. Khanna and Brasseur (1998) explain LES's popularity thus, "… *large-eddy simulation provides the full space-time evolution of the larger-scale motions within the atmospheric boundary layer – information inaccessible with any other technique*." Fedorovich (2004), however, recognized the dangers in substituting LES for observations. He states that, "… *analyses and interpretations of these new numerical data will not be conclusive and complete without new laboratory and field experimental data available for verification of numerical simulations*." LES has already been used as a surrogate for field experiments. Examples include studies of plume behavior (Dosio et al. 2003; Kim et al. 2005), analysis of large-scale atmospheric structures associated with different atmospheric stability states (Khanna and Brasseur 1998), and the effects of near-surface coherent structures on vertical flux of horizontal momentum (Foster et al. 2006).

Stevens and Lenschow (2001) explored how one could decide if such applications are appropriate. They proposed two conjectured conditions that, if either one were satisfied, would justify the use of LES as a practical experimental tool. The Stevens and Lenschow (2001) conjectures are: 1) "*The SGS* [subgrid scale] *model used in LES is a faithful reproduction of reality*." or 2) "*The statistics of the low-frequency modes that are explicitly calculated by LES are not sensitive to errors in the parameterization of SGS effects*."

Detailed experimental evidence necessary for rigorous verification of the first conjecture is generally unavailable (see e.g. Fedorovich 2004), so simulation success is often measured with more general comparisons between major simulated features of flow or temperature fields and those observed in field campaigns (e. g. Berg and Zhong 2005; Chen et al. 2004), or by comparisons of observed and modeled average (spatial or temporal) profiles of easily measured low-order moments of basic flow parameters (e. g. Nieuwstadt et al. 1991). The model results are then used to draw conclusions about flow details, or more complicated processes involving higher-order quantities that cannot be measured (e. g. Moeng and Wyngaard 1986).

The second, less restrictive, conjecture is essentially a restatement of the underlying premise of LES, i.e. that energy in unresolved scale motions is much less than that in the resolved motions, as is often tacitly assumed. Evidence presented here suggests that its truth cannot be taken for granted, because the larger scale flow features (i. e. Stevens and Lenschow's low spatial frequency modes) do change when the subfilter (i.e. small spatial scale) model changes.

Innovative field measurements from the Horizontal Array Turbulence Study (HATS, Horst et al. 2004) give promise for checking the first Stevens and Lenschow (2001) conjecture that an SGS model provides a faithful reproduction of reality. The HATS experiments could reveal relationships between observed subfilter turbulence and the corresponding filtered motions in real geophysical flows and thereby provide a better picture of relationships between filtered and unfiltered motions. This, in turn, can lead to more realistic models of subfilter behavior (e. g. Kleissl et al. 2004; Chen and Tong 2006; Porté-Agel et al. 2001; Wyngaard 2004; Hatlee and Wyngaard 2007).

Here, we simulate a neutrally-stable boundary layer flow and extend the earlier analyses of Chow et al. (2005) and Ludwig et al. (2006) by examining the influence of turbulence models and spatial resolution on resolved patterns of variables. This neutral boundary layer flow is similar to the one analyzed by Lin et al. (1996) and Foster et al. (2006) who obtained bulk LES results that were consistent with direct numerical simulations (DNS) by Coleman et al. (1990).

2. Flow simulation examined

2.1 ARPS code

The Advanced Regional Prediction System (ARPS) is a well documented code that can be applied to LES problems (Xue et al., 1995, 2000, 2001). It was modified by Chow (2004) to include new subfilter-scale models. Table 1 summarizes how ARPS was used here with two grid spacings: coarse 32 m horizontal and fine, 8 m.

1. Corresponding author: Francis L. Ludwig, Environmental Fluid Mechanics Laboratory (MS 4020), Stanford University, Stanford, CA 94305, phone: 650-721-2680, fax: 650-725-9720, e-mail:fludwig@stanford.edu

Table 1: Characteristics of ARPS as used in this study

Characteristic	Description
Spatial discretization	Arakawa C grid
Number of grid points:	
coarse grid	40x40x40
fine grid	160x160x160
Horizontal spacing:	
coarse grid	32 m
fine grid	8 m
Vertical spacing (stretched):	
coarse grid near surface	~10 m
near top	~65 m
fine grid near surface	~5 m
near top	~16 m
Temporal discretization (both grids): Large step	0.5 s, 2nd-order leapfrog
Small step (acoustic mode)	0.05 s, 1st-order forward–backward
Horizontal advection	Fourth order
Vertical advection	Second order
Boundaries:	
Lateral	Periodic
Top	Rigid free slip
Bottom	Rigid free slip with surface drag
Spatial computational mixing	Fourth order
Subfilter turbulence models	As discussed in text

2.2 Subfilter-scale turbulence models tested

Chow (2004) and Chow et al. (2005) give detailed descriptions of the particular models used to obtain the results presented here, so the following description is very brief. LES separates larger, resolved scales from smaller, unresolved scales with a spatial filter (usually related to the mesh size). Estimating spatial derivatives from an array of point values introduces further implicit spatial filtering. The implicit discretization and the explicit LES filtering lead to three categories of flow energy: 1) wholly resolved, 2) resolvable subfilter-scales (RSFS) smoothed by filtering and 3) completely unresolved subgrid motions. Knowledge of the explicit filter permits RSFS motions to be mathematically reconstructed and used to model resolved motion effects, but it is seldom that they can be exactly reconstructed. Unresolved subgrid-scale (SGS) motions are modeled separately, usually with an eddy-viscosity approach (Gullbrand and Chow, 2003).

The filtered, incompressible Navier-Stokes equations with continuity on a discrete mesh include the stress terms, $\partial\tilde{\tau}_{ij}/\partial x_j$ to be modeled. Turbulent stresses are defined:

$$\tau_{ij} = \overline{\tilde{u}_i\tilde{u}_j} - \bar{\tilde{u}}_i\bar{\tilde{u}}_j = \left(\overline{\tilde{u}_i\tilde{u}_j} - \bar{\tilde{u}}_i\overline{\tilde{u}_j}\right) + \left(\overline{\tilde{u}_i}\overline{\tilde{u}_j} - \bar{\tilde{u}}_i\bar{\tilde{u}}_j\right) = \bar{A}_{ij} + B_{ij} \quad (1)$$

Conventional notation is used; x's for coordinates; u's for wind components. Repeated subscript indices indicate summation; tildes and over-bars denote discretized and filtered quantities, respectively. Tilde operators are implicit in the finite difference calculations and are ignored in the numerical implementation. The explicit filter (over-bar) is applied only when calculating subfilter scale (SFS) stress terms (Chow et al. 2005). $\bar{A}_{ij}$ and B_{ij} represent the parenthesized terms directly above in Equation 1, which follows the example of Carati et al. (2001) by separating stress into: $\bar{A}_{ij}$, the SGS stress that depends on unresolved motions, and B_{ij}, the resolved subfilter-scale stress (RSFS) composed of resolved filtered motions. In theory, B_{ij} can be reconstructed from filtered fields, but closure models must represent the SGS components in $\bar{A}_{ij}$, because $\overline{\tilde{u}_i\tilde{u}_j}$ cannot be calculated from grid point values. The widely used eddy viscosity concept serves to model $\bar{A}_{ij}$:

$$\bar{A}_{ij} = -2\nu_T\,\overline{\tilde{S}_{ij}} = -\nu_T\left(\frac{\partial\overline{\tilde{u}_i}}{\partial x_j} + \frac{\partial\overline{\tilde{u}_j}}{\partial x_i}\right) \quad (2)$$

The SGS eddy viscosity is ν_T. $\overline{\tilde{S}_{ij}}$ is the resolved strain rate tensor. Chow et al. (2005) determined eddy viscosity ν_T from one of two models: 1) the Smagorinsky model or 2) the dynamic Wong-Lilly (DWL) model (Wong and Lilly 1994). The Smagorinsky (1963) model uses the square of the grid spacing Δ_g^2 and the Smagorinsky coefficient C_S:

$$\nu_T = \left(C_S\Delta_g\right)^2\left(2\bar{\bar{S}}_{ij}\bar{\bar{S}}_{ij}\right)^{1/2} \quad (3)$$

The Smagorinsky model is similar to commonly-used eddy viscosity closures based on turbulent kinetic energy (e. g. the TKE 1.5-order model), but its formulation is more straightforward and sidesteps debate about appropriate coefficient values for the TKE equation (see e. g. Deardorff 1971; Takemi and Rotunno 2003).

The DWL model (Wong and Lilly 1994) substitutes a dynamic expression (Germano et al. 1991, Lilly 1992) for eddy viscosity:

$$\nu_T = C_S^{2/3}\Delta^{4/3}\varepsilon^{1/3} = C_\varepsilon\Delta^{4/3} \quad ; \quad (4)$$

C_ε replaces the Smagorinsky coefficient (C_S) and turbulent dissipation rate (ε), thereby avoiding requirements that ε equal the SGS rate of energy production, and that effective grid cell spacing Δ be defined exactly – the product term $C_\varepsilon\Delta^{4/3}$ is calculated dynamically (Germano et al. 1991) from Lilly's (1992) least squares approximation.

Following Stolz and Adams (1999), RSFS motions and associated stresses in B_{ij} are reconstructed using van Cittert's (1931) iterative inverse filter approximation for deconvolution of the RSFS terms. Recovered unfiltered fields $\tilde{u}_i$ are substituted in the RSFS stress tensor

$B_{ij} = \overline{\tilde{u}_i \tilde{u}_j} - \bar{\tilde{u}}_i \bar{\tilde{u}}_j$. Van Cittert's approximate deconvolution method (ADM) recovers velocity to a known order of accuracy; different reconstruction levels yield different B_{ij} models when combined with the separately modeled SGS stresses. Each RSFS/SGS combination yields a mixed model for total turbulent stress (cf., Bardina et al. 1983).

The six models used here are: 1-3) three models that combine Wong-Lilly with van Cittert reconstruction to accuracies of zeroth, first and fifth order, 4) the modified Clark (Clark et al. 1977) model that combines the Wong-Lilly model with reconstruction using Taylor series, 5) the dynamic Wong Lilly without reconstruction, and 6) the Smagorinsky model without reconstruction. Dynamic reconstruction models (1-3) are denoted by reconstruction level, DRM-ADM0, DRM-ADM1and DRM-ADM5.

A near-wall stress model supplements the dynamic SGS turbulence models near the surface in both the 32- and 8-m simulations. It accounts for stress induced by filtering and large grid aspect ratio effects near the solid lower boundary (see Dubrulle et al. 2002, Nakayama et al. 2004, Brown et al. 2001, and Chow et al. 2005), which the dynamic eddy-viscosity procedure fails to do. The near-wall model is not used with the Smagorinsky closure because that model is already overly dissipative (see Chow et al. 2005, Fig. 4). The near-wall model derives from Brown et al. (2001). It adds drag to account for roughness and grid aspect ratio effects and is considered part of the SGS stress. The resulting stress appears as:

$$\tau_{i,near-wall} = -\int C_c a(z) \left|\bar{\tilde{u}}\right| \bar{\tilde{u}}_i dz \qquad (5)$$

Nakayama and Sakio (2002) and Nakayama et al. (2004) provide a theoretical basis for this near-wall model of rough boundary flow. The shape function *a(z)* tapers near-wall stress smoothly to zero at the top of (and above) the near-wall region ($z \lesssim 4\Delta x \approx 128$ m for the coarse grid and ≈ 32 m for the fine); C_c depends on grid aspect ratio and falls between 0.4 and 0.8 (Chow et al. 2005),

Earlier simulation results (Chow et al. 2005) showed that the theoretical log profile was better reproduced by the dynamic and Modified-Clark models than by the Smagorinsky; the DRM framework consistently produces better agreement with a log profile in terms of mean quantities and turbulent stress behavior.

2.3 Neutral atmospheric boundary layer test case

Chow et al. (2005) used the six subfilter models to simulate large-scale, neutral, rotation-influenced, boundary layer flow with ARPS. The same flow has been examined by others (e.g. Andren et al. 1994; Foster et al. 2006). This 10 m s^{-1} westerly geostrophic flow is driven by a constant pressure gradient and Coriolis parameter $f = 10^{-4}$ s^{-1} (~ 43° north latitude). Flow was initialized with small perturbations on the analytical Ekman spiral solution, so that a fully turbulent flow developed. Parameterized surface momentum fluxes approximate a rough lower boundary. The Chow et al. (2005) results with a 32-m grid served as the basis for the analyses presented by Ludwig et al. (2006). Here, we examine new variables on the 32-m grid and look at results from new 8-m grid runs with Smagorinsky and DRM-ADM0 models. The Smagorinsky model was chosen for these fine scale comparisons, because it, or the closely related TKE model, have been so widely used in previous studies. The simplest of the dynamic reconstruction models, DRM-ADM0, was chosen to represent that category.

3. Results

3.1 Variations with height

3.1.1 Vertical velocity

Continuity requires that the layer mean vertical velocities (not shown) equal zero. Statistical tests reported by Ludwig et al. (2006) confirmed that none of the subfilter models produced coarse grid layer averages that differed significantly from zero. However, the variations, as measured by the standard deviation of vertical velocity, σ_w, with height revealed by LES on a 32-m grid were significantly different for many model pairings. Figure 1a shows results for the six models tested with the coarse grid LES. The largest σ_w exceeds the smallest by about 0.05 m s^{-1} at most heights. Peak σ_w values are at different heights, but most are between about 125 m and 225 m.

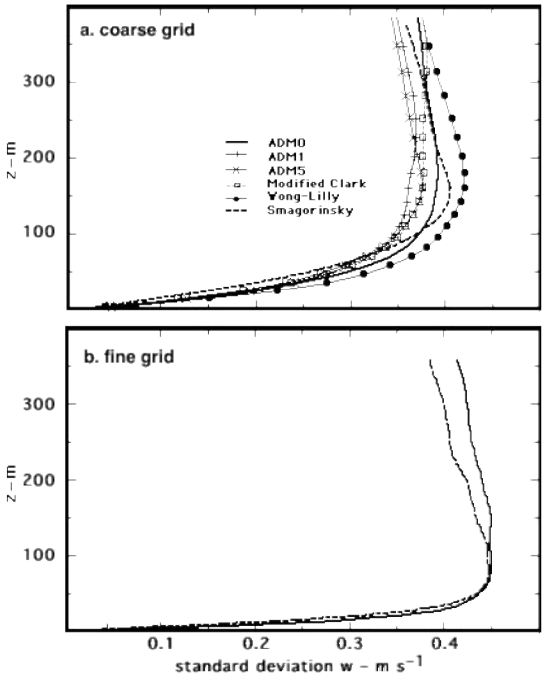

Figure 1. Standard deviation of vertical velocity versus height for coarse and fine grid simulations.

Figure 1b shows the σ_w profiles for the DRM–ADM0 and the Smagorinsky models on the 8-m grid. The fine grid simulations produce larger w fluctuations for the same models (Figure 1a) than those on the coarse grid. For both

fine grid DRM–ADM0 and Smagorinsky model runs, σ_w reaches a peak value of about 0.45 m s^{-1} at about 75 m altitude, while the coarse grid peak values are about 0.39 and 0.40, respectively and are at about twice the altitude as those for the fine grid.

Large σ_w values can be produced by: 1) up and down motions distributed randomly over the grid points, or 2) extensive, organized updrafts and downdrafts, or 3) a combination of the first two. Ludwig et al. (2006) showed that Type 2) dominated for the coarse grid simulations. Later, it will be shown that that is also the case for the fine grid results.

3.1.2 Vertical flux of streamwise momentum

Foster et al. (2006) applied a well-resolved (6.25 m horizontal and vertical grid spacing) TKE closure LES model " *… to explore the relationships between coherent structures and the vertical momentum flux*." Given the differences observed in coherent structures in the vertical motion field reported by Ludwig et al. (2006), it seemed reasonable to study how the Foster et al. (2006) results might have been affected by choice of subfilter model and by spatial resolution.

Foster et al. (2006) categorized $\overline{w'u'}$ momentum transport according to "quadrant," where larger (smaller) than average components are denoted by + (–) superscripts. Downward transport occurs as *ejections* (w^+u^- in quadrant 2) and *sweeps* (w^-u^+ in quadrant 4) and *upward* u–momentum flux in quadrant 1 (w^+u^+) or quadrant 3 (w^-u^-). Figure 2 presents profiles of area covered and mean fluxes for 32 m resolution simulations (normalized by the squared fiction velocity, u_*) for ejections, sweeps and upward flux. Figures 2a-c show notable differences between coarse-grid flux profiles for the different models, especially in the ejection category. Generally, the Wong-Lilly model produces larger average ejection fluxes than the others. Differences in the sweep results are somewhat less pronounced. The largest averages of upward flux are generally associated with the Wong-Lilly results and the smallest average upward flux values with the two higher-order reconstruction models. Figures 2d-f show fractional areas occupied by different flux categories. The domain tends to be more or less evenly divided among ejections, sweeps and the two upward flux quadrants. Above about 50 m, the largest area covered by a model differs from the smallest area by less than five percent in a particular flux category. Larger differences occur near the surface.

Figures 3a-c compare average ejection, sweep and upward streamwise momentum fluxes obtained with the Smagorinsky and DRM-ADM0 subfilter models on both the 8-m grid and 32-m grids. The fine resolution flux maxima are nearer the ground than for the coarse resolution, resulting in stronger gradients in the lowest 50 m for all three momentum flux categories. Above about 100 m, the fine resolution results, especially for upward flux events, for DRM-ADM0 and Smagorinsky models are similar both to each other and to their coarser resolution

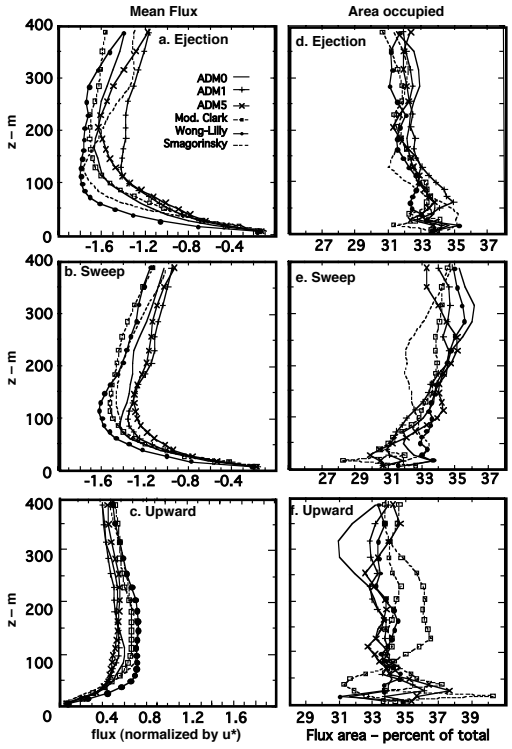

Figure 2. Mean Fluxes (normalized by u_*) and percentage of the area occupied by different flux types for coarse grid results.

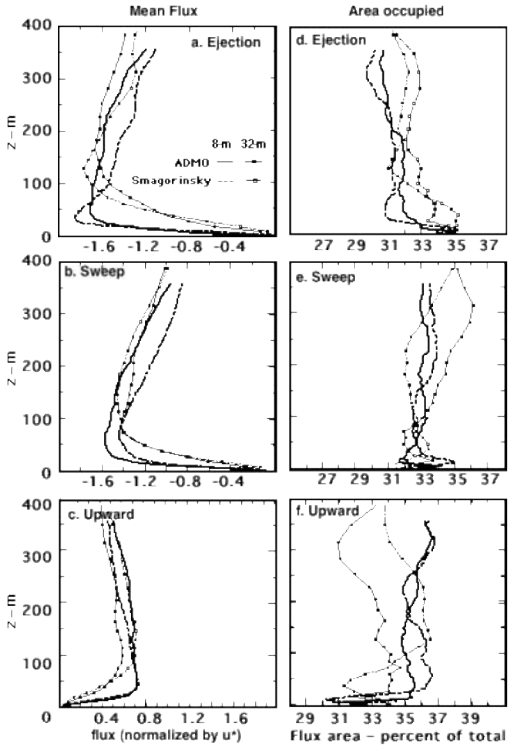

Figure 3. Comparisons of fine and coarse grid mean fluxes (normalized by u_*) and percentage of the area occupied by different flux types.

counterparts. Furthermore, the higher altitude fine scale results tend to fall within the range spanned at the same altitude by all six models used at 32-m resolution.

The areas occupied by ejections, sweeps and upward momentum flux (Figures 3d-f) also show sharper near-surface gradients with the fine resolution than with the coarse. Furthermore, the spacing between the two model profiles is smaller for the fine grid results than for the coarse at most altitudes, indicating better agreement between the two models with regard to areas occupied by ejections, sweeps and upward flux. Given the premises of LES, it is reasonable that subfilter model effects are greater when resolution is poor and more energy goes unresolved.

3.2 Effects of models on horizontal distributions

3.2.1 Vertical velocity

The standard deviation profiles in Figure 1 show that different models can produce profiles with important differences. As noted earlier, even means and standard deviations that are statistically indistinguishable may have been calculated from populations with very different spatial correlations so that the individual values are organized very differently in space. For example, Ludwig et al. (2006) showed that the spatial arrangements of vertical motion vary with altitude and subfilter model, although all the layer means were zero. Figure 4 shows that the standard

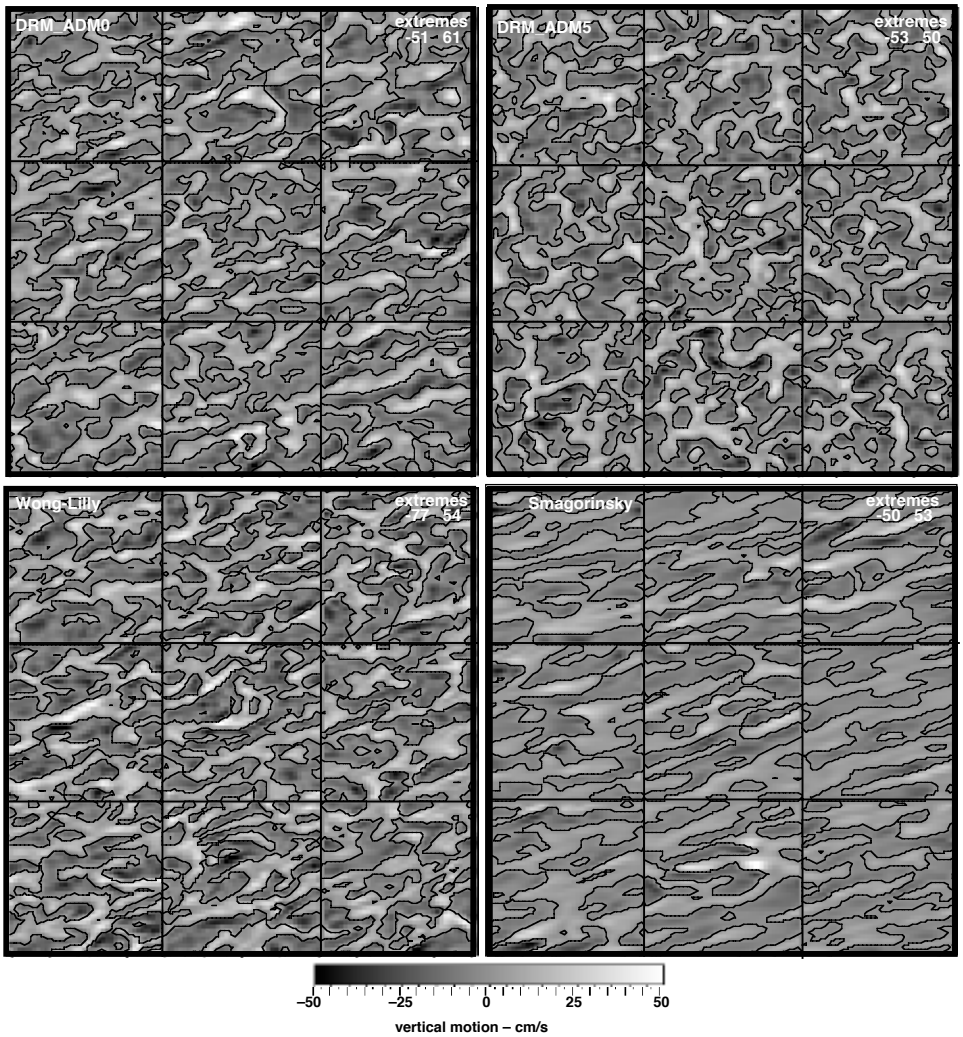

Figure 4 **Vertical motions produced at 15 m on the 32-m grid by four subfilter models (large squares) at nine different times (small squares).** The small squares at upper left are the earliest of the nine times shown for that model; the latest is at the lower right. Extreme values for each model are shown in the corner of the large squares. Solid lines in the small squares mark the boundary between upward and downward motion (w=0)

deviation profiles in Figure 1, that differ both with resolution and among the subfilter models produce noticable differences in spatial patterns at 15 m height.

Figure 4 (a different display of the same data used in Figure 2 of Ludwig et al. 2006) shows sequences of 32–m grid vertical velocities at 15 m altitude. Each large square shows results for one of the models; the nine small squares in each large square show individual snapshots from 280 000 s to 300 000 s. Light grays represent upward motion and dark grays downward. The black isotach for w=0 separates upward from downward motion. Extreme values are shown in the corner of each model square. There is variability both among models (large squares), and from one time to another for the same model (small squares).

The most striking difference between the Smagorinsky model and others is the nature of the patterns. Smagorinsky, far more than the others, produces long lines of upward motion separated by lines of downward motion. There are only hints of such linearity in the patterns produced by the DRM-ADM5. Although other models have some linear structure, their lines are not nearly so pronounced as in the Smagorinky results. Ludwig et al. (2006) showed (their Figure 3) that the Smagorinsky model's patterns differed less from the others at higher altitudes .

Figure 5 shows vertical motion patterns at 9 m and 152 m when 8-m grid spacing was used with the DRM-ADM0 and Smagorinsky models. A color scale is used instead of the grey in Figure 4, because the finer scale w=0 isotachs were too intricate to display properly. As with the coarser resolution, the Smagorinsky model produces more elongated patterns at a low altitude (9 m) than does the DRM-ADM0. The elongated elements in the pattern are much more closely spaced than those found with the coarse grid. Qualitatively, the difference between models is not as pronounced as those in Figure 4. As with the coarser simulations, the areas of contiguous regions of upward and downward motion are greater at the higher altitude.

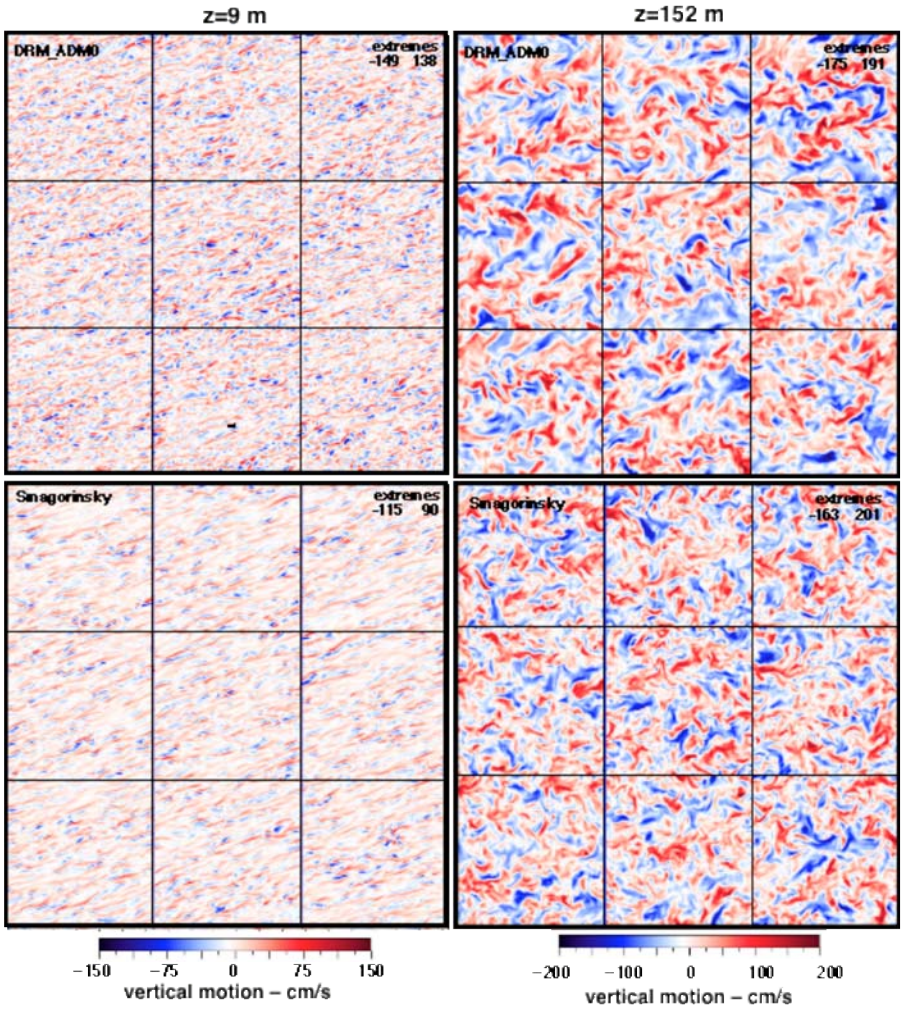

Figure 5. Vertical motions at 9 m and 162 m on the 8-m grid by two subfilter models at nine times (small squares).

The correlograms in Figure 6 are a different, more quantitative way of displaying the tendency for the formation of patterns in the field of vertical motion. Correlograms are shown in Figures 6a-c for all six models tested with 32–m resolution and at three heights (15, 47 and 162 m). They illustrate the gradual changes with height. The isopleths are correlation coefficients between vertical velocity at a point in the center of each pattern and all the surrounding points, as derived from the complete sample of all 27200 (40×40×17) values at each elevation. Correlation isopleths ≥ 0.2 are shown at intervals of 0.2. The spatial scale is given in Figure 6a.

There is a tendency at the 15 m and 47 m heights (Figures 6a and 6b) for most models to have correlations at a given distance from the reference point that are greatest along a line oriented from about 12° to 18° counter-clockwise (CCW) from the x axis. All structures, excepting those from the DRM-ADM5 model, are less elongated at the 162 m level, with smaller major to minor axis ratios than at the lower levels. At 162 m (Figure 6c), the Smagorinsky correlogram resembles those of the other models, except for its smaller extent. The area within the 0.2 correlation isopleth increases for every model, indicating larger organized structures at 162 m than at the lower levels. The differences among models, even aloft, indicate that they do not satisfy the second Stevens and Lenschow (2001) conjecture. The differences tend to confirm Juneja and Brasseur's (1999) opinion that errors near the surface can infect the entire flow field.

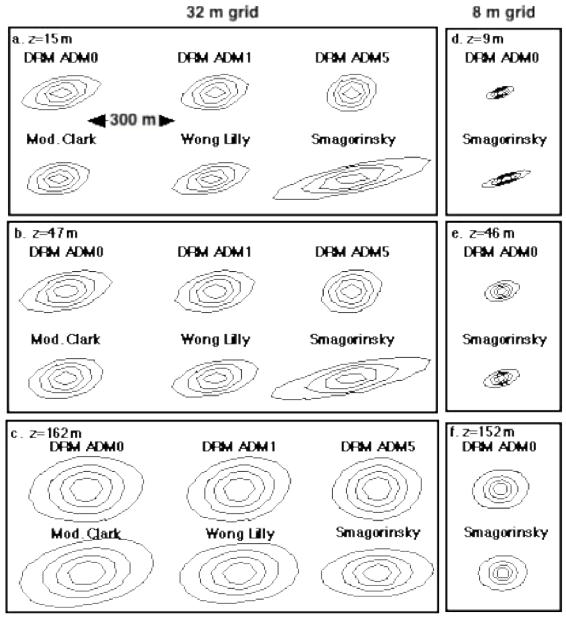

Figure 6. Correlograms of vertical velocity for 32-m (a-c) and 8-m grid (d-f) LES for six subfilter models. Isopleths are for correlations of 0.2 (largest curves), 0.4, 0.6 and 0.8 (smallest curves); spatial scale is shown in panel a.

The correlograms in Figures 6d-f are derived from 435200 (160×160×17) values at each elevation from 8-m resolution DRM-ADM0 and Smagorinsky model simulations. The 9 m elevation correlograms (6d) confirm that the Smagorinsky patterns are appreciably more elongated than the DRM-ADM0. The models differ less at 46 m, and at 152 m, both patterns are only slightly elongated, but DRM-ADM0 patterns are noticeably larger than the Smagorinsky. Both models produce smaller up- and downdraft areas than at similar heights for coarse simulations. The coarse resolution patterns are more than three times larger in linear dimension at the lowest altitude and about twice as large near 150 m. The finer resolution leads to closer spacing of smaller contiguous areas.

The differences in the structure of vertical motions from each turbulence model can be compared with similar flows in the open atmosphere. Neutrally stratified flow above a rough flat surface occurs over water when air and water temperatures are equal so there is no surface heat transfer. Woodcock's (1942) observations of soaring herring gulls (summarized in Figure 7) provide a test for the realism of model results. Gull behavior shows that updrafts extensive enough to support their soaring did not occur during stable or neutral conditions. The approximate conditions simulated here are indicated in Figure 7 (assuming Woodcock measured wind speeds at ~10 m). Long lines of updraft (Smagorinsky) are inconsistent with Woodcock's observations. Gulls only soared in long lines (like the linear structures of the Smagorinsky model) when stratification was more convective and wind speed higher.

3.2.2 Ejections, sweeps and upward fluxes of streamwise momentum

Foster et al. (2006) used LES to assess the relative importance of ejections and sweeps in the vertical transfer of streamwise (u) momentum. The differences in the average area occupied by ejections, sweeps and the upward fluxes shown in Figure 2 and 3 suggest that some conclusions drawn by Foster et al. (2006) may have been affected by their choice of subfilter model.

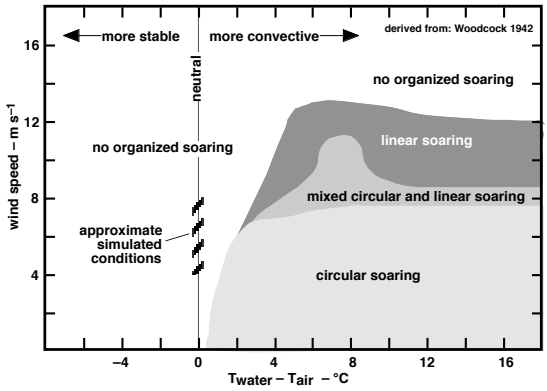

Figure 7 Woodcock's (1942) observations of winds, sea–air temperature differences and the associated soaring patterns of herring gulls.

Figures 8 and 9 show the areas occupied by ejections, sweeps and upward momentum flux for the last nine snapshots from the 32 m grid, for four models at two heights. The differences in the general shapes of ejection, sweep, and upward flux areas are apparent, especially at the lower altitude. Figure 8 shows that three of the four models shown have "streaky" ejection (black areas in the figure) patterns at 15 m. The DRM-ADM5 and modified Clark (not shown) are exceptions. Most of the models do not organize the sweeps (grey areas) into lines that are as long and continuous as the ejections. Regions of upward flux (white) often enclose a sweep, except for the Smagorinsky model, whose elongated sweeps are often separated from ejections by a line of upward flux. All streaky patterns are rotated CCW from the geostrophic, west-to-east flow.

At 162 m (Figure 9), the contiguous areas of ejections, sweeps and upward fluxes are larger for any given model than for the same model at the lower altitude. The elements of the Smagorinsky patterns are smaller than those of other models at this higher altitude. Sweep areas tend to be longer than wide, but without the uniform orientation that gives the strong sense of streakiness seen at the lower altitude. All the models produce ejection, sweep and upward flux features that are more continuous in the streamwise direction than in the spanwise.

Figure 10 shows the 8-m grid ejection/sweep patterns at two altitudes for the DRM-ADM0 and Smagorinsky models. The bottom row shows patterns obtained by Foster et al. (2006) at two similar altitudes. Their patterns have been graphically modified to make it easier to compare them with our results. Taking advantage of periodic boundary conditions, a duplicate of a Foster et al. (2006) figure was placed above the original to form a 2 by 3 km pattern that was then rotated 18° CCW to offset the rotation introduced by Foster et al. (2006). Finally, 1.2 km squares

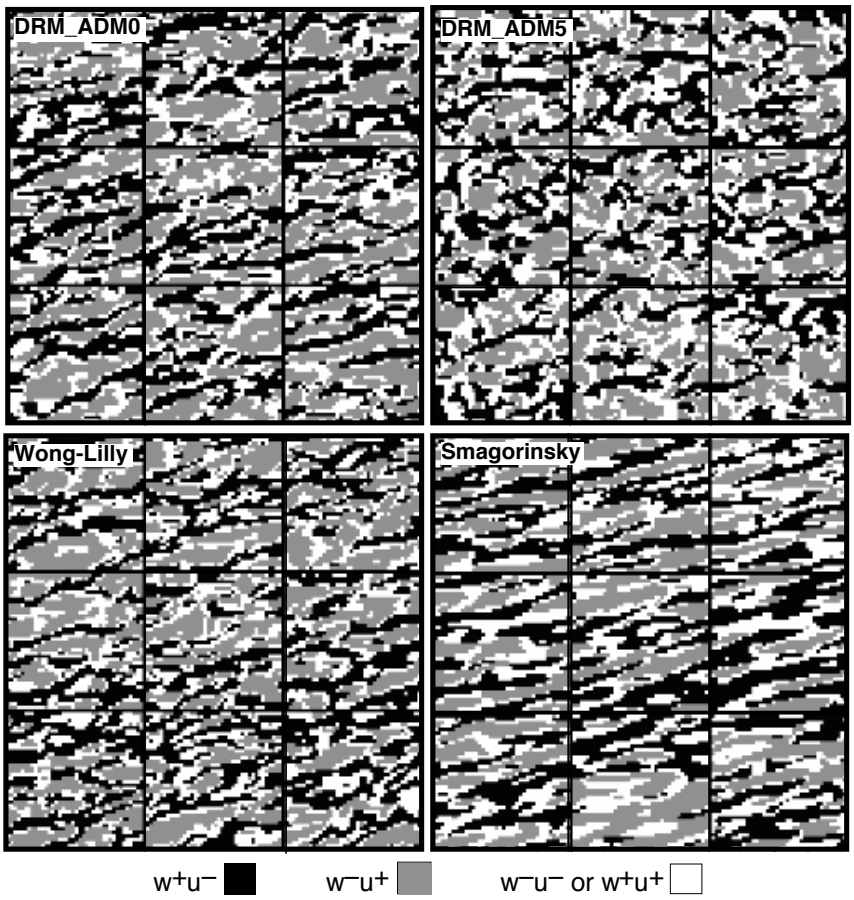

Figure 8 Distribution of areas on 32-m grid occupied by ejections, sweeps and upward momentum flux at 15 m for four subfilter models.

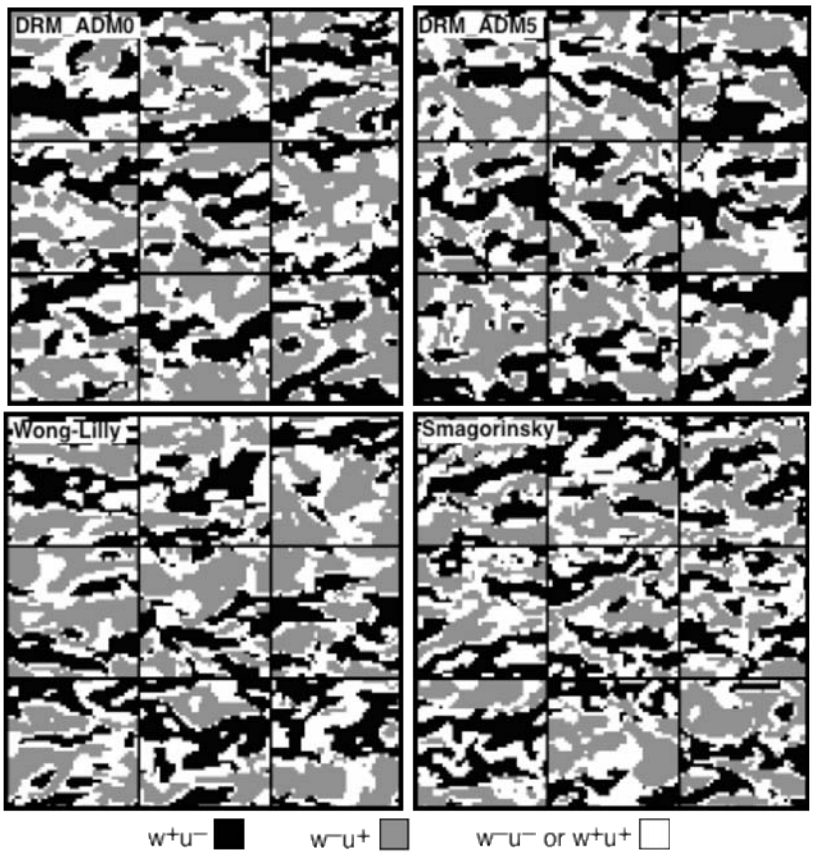

Figure 9 Distribution of areas on 32-m grid occupied by ejections, sweeps and upward momentum flux at 162 m for four subfilter models.

were extracted and plotted in Figure 10. These small squares represent different areas from the same snapshot, rather than snapshots at different times.

Qualitatively, the Foster et al. (2006) results look more like the Smagorinsky patterns at the lower altitude, and more like the DRM-ADM0 at the higher altitude. Regardless of subfilter model, contiguous areas are larger for coarse grid simulations (Figures 8 and 9) than for the fine grid (Figure 10) at a similar altitude. Also, fine grid results differ less between the two subfilter models than for the coarse grid, where distinct differences between the models were observed, especially near the surface. Finally, the general appearance of the fine grid snapshots at the lower heights changes little with time, probably because there are many small structures in the domain, with little relative variation in their number from one realization to another, whereas only a few large coarse grid structures fit in a frame, so their numbers can easily differ by a factor of two or more from one time to another.

3.2.3 Length of zero flux isopleths

One possible answer to the question of how the observed pattern differences are related to subfilter-scale model effects comes by analogy with what Sreenivasan et al. (1989) observed and theorized about the behavior of interfacial surfaces in turbulent fluids. They related microscopic details of the interfaces between mixing layers to the macroscopic fluxes between regions. Among other conclusions, they noted that "*an interesting interpretation is that the turbulent surfaces at the 'microscopic' level adjust themselves in such a way that the 'macroscopic' fluxes are independent of viscosity*." and, "*In all practical circumstances, the scale range over which the power laws hold … is bounded by cutoffs at both ends. For surfaces in turbulent flows, the outer cutoff is expected to occur at scales comparable to the integral scale … of the turbulence, while the inner cutoff occurs at the smallest dynamical scale. For vorticity interfaces, the appropriate inner scale is the Kolmogorov scale* η *… "* The Kolmogorov scale depends on kinematic viscosity. Another important characteristic of the interfaces is that the surface area of the interface increases as the convoluted distortions are extended to smaller scales. In essence, Sreenivasan et al. (1989) argue that the transfer of momentum and other scalars is accomplished by microscale processes across the thin layers associated with intricate interface shapes. A viscosity change alters the small scale cutoff and changes the intricacy of the interfaces, and hence changes the overall surface area where microscale processes actively mix scalars.

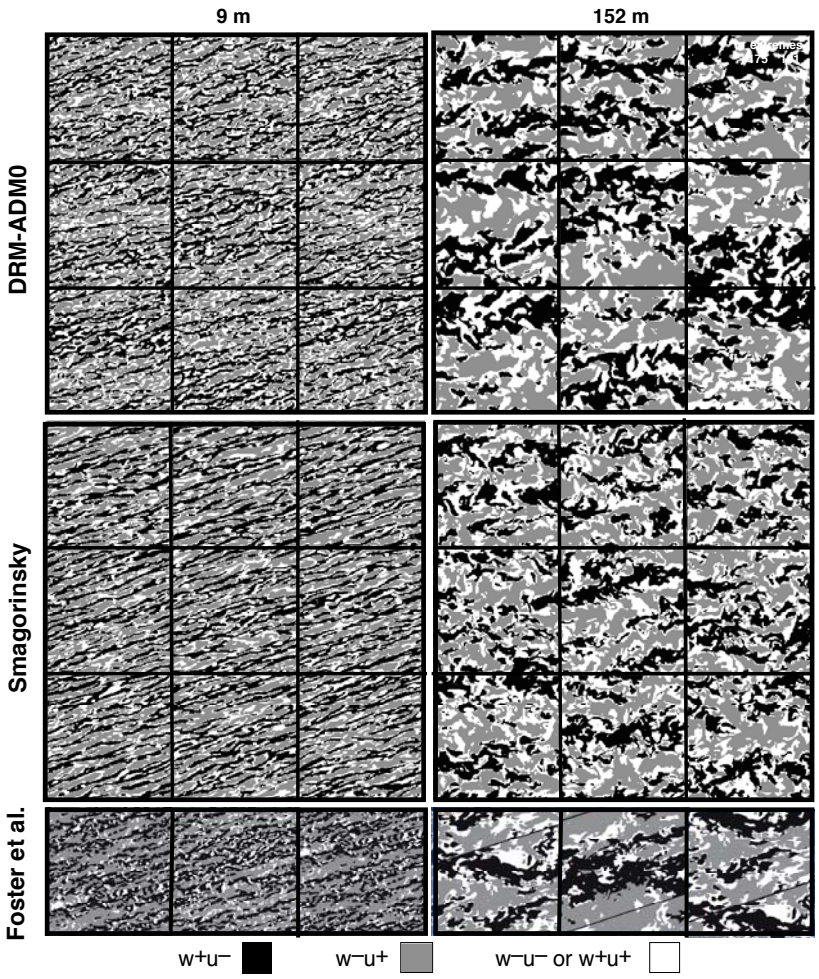

Figure 10 Distribution of areas on 8-m grid occupied by ejections, sweeps and upward momentum flux at 15 m and 162 for the DRM-ADM0 and Smagorinsky models. Foster et al. (2006) results at approximately same scale and heights are also shown (see text for explanation).

Large-eddy simulations differ from the situation described by Sreenivasan et al. (1989) in that the small-scale end of the cascade is fixed by the filter and/or grid scales. Furthermore, the fixed small scale of LES may not support the intricate interfaces found in real fluids. However, the idea that total surface area may adjust to accommodate "viscosity" changes may apply in LES, where different subfilter models generate different "viscosities." The LES attempts to produce the interface necessary for proper transfer of momentum in the turbulent flow by generating different shapes for resolved features in order to provide more, or less, interface area between regions of upward and downward momentum flux.

The above reasoning led to calculation of the lengths of w'u'=0 isopleths (the 2-dimensional manifestation of the 3–d interfacial surface discussed above). The lengths were estimated by counting pairs of adjacent grid points of opposite sign and assuming that an isopleth segment of length equal to the grid size passes between these points of opposite sign. Differences in model "viscosities" should lead to different isopleth lengths. Larger values of the effective model viscosity should be associated with shorter isopleths.

Figure 11 shows isopleth lengths for 17 snapshots at two altitudes, 15 m (•) and 162 m (×), on the 32–m grid for four subfilter models. Each point in Figure 11 represents the total w'u'=0 length for a particular snapshot. For reference, the maximum length possible (a checkerboard of alternating signs) is 96 km. The ordinate scale on the right shows the percentage of this maximum length. Rectangles in Figure 11 span upper and lower quartiles; a horizontal line in the rectangle marks the median of the 17 lengths, while shaded regions span the 95–percent confidence interval for the median (Velleman 1997). Medians differ significantly when their confidence intervals do not overlap.

All models display considerable variation in zero isopleth length from one snapshot to another. Of the models shown, only the Smagorinsky model differs significantly from all the rest at 15 m. Smagorinsky w'u'=0 isopleths are much shorter than the others, consistent with the notion that the Smagorinsky model's larger eddy viscosities lead to reduced interfacial intricacy and result in smoother large scale structures. Smagorinsky w'u'=0 isopleth lengths change little with distance from the surface, while the other models produce substantially shorter isopleths (indicative of larger, smoother structures) at higher levels. Higher up, Smagorinsky isopleths are longer than all but the DRM–ADM5.

Lengths of the w'u'=0 isopleths produced by the DRM-ADM0 and Smagorinsky models on the 8-m grid are shown in Figure 12 for four different altitudes. The smaller grid size allows for finer scale detail to be represented, leading to much longer isopleths than their coarse grid counterparts. The maximum length for the fine scale is 384 km. Near the surface, the Smagorinsky model produces shorter isopleths than does the DRM-ADM0, but the Smagorinsky isopleths are longer aloft. Differences between model medians are significant at all altitudes shown, and become more so above 27 m.

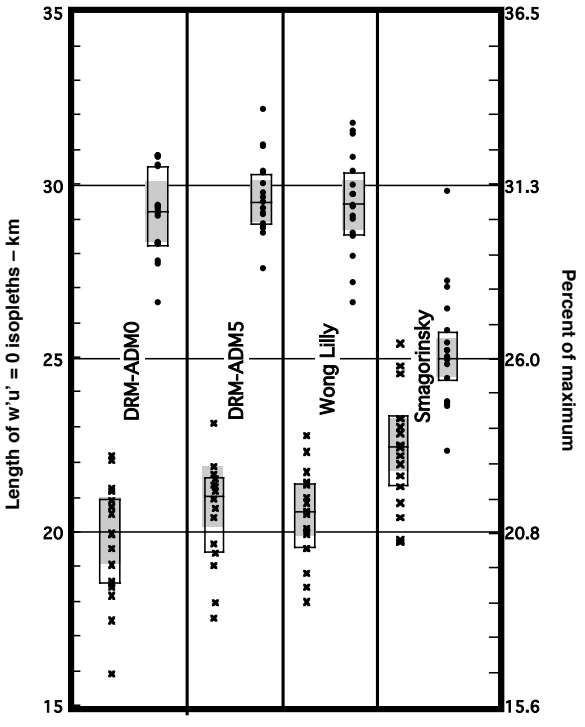

Figure 11 Lengths of w'u'=0 isopleths produced by 32 m grid simulations with four subfilter models at 15 m (•) and 162 m (x). Lengths are shown for each model's 17 snapshots. Boxes extend from lower to upper quartile; shaded regions span the 95 percent confidence about the median (line within box).

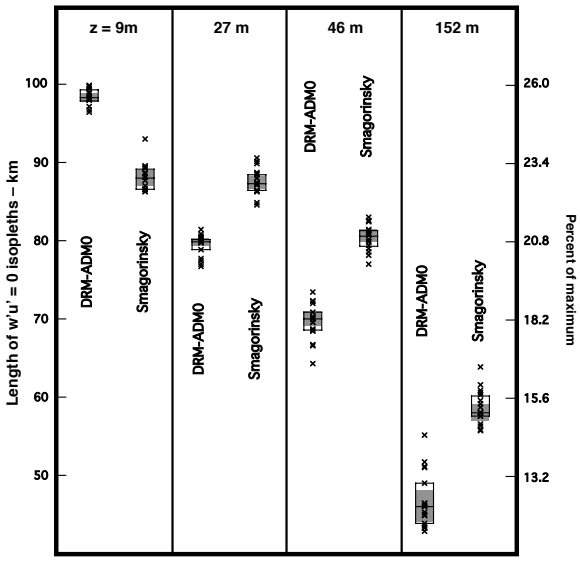

Figure 12 Lengths of w'u'=0 isopleths produced by 8 m grid simulations with two subfilter models at four heights.

Note that the similar appearing patterns of ejections, sweeps and upward flux in Figure 10 have significant differences in the lengths of their zero momentum flux isopleths. The results in Figures 11 and 12 indicate that models can produce significantly different features at resolved scales, even well away from the surface.

4. Conclusions

4.1 Summary of findings

Changes in subfilter model and resolution produce important differences in the bulk effects and the nature of the resolved flow.

As measured by correlograms, features in the vertical motion patterns for a given model and resolution tend to grow larger in area and less elongated in shape with height. At a given altitude, finer resolution reduces the extent of the spatial correlation in the vertical motion patterns, indicating that the active eddies can be smaller when the resolution is improved. At low altitudes, the linear extent of the Smagorinsky patterns exceeds that of the other models, but the relationship is generally reversed at higher altitudes. At a given altitude, features in the patterns of ejection, sweep and upward flux are smaller for finer resolution simulations.

Important differences among the models are found in momentum flux profiles for sweeps, ejections and upward flux. Fine grid simulations produce larger σ_w for the same models (Figure 1) than those on the coarse grid, and the peak σ_w values on the coarse grid are about twice as far from the surface as they are for the fine grid.

Patterns of upward and downward motion produced in coarse grid simulations with the Smagorinsky model do not agree with what has been observed in neutral atmospheric flows over the similarly flat, featureless ocean.

Lines of w'u'=0 separating upward flux from downward are significantly shorter for Smagorinsky coarse grid simulations near the surface than they are for the other models at the same resolution, indicating a less convoluted interface. At higher altitudes, the Smagorinsky w'u'=0 lines are longer (more convoluted) than the others. Lengths decrease with altitude for all models. Finer resolution allows for more convoluted, and hence longer zero flux isopleths.

4.2 Implications

The results presented above suggest that neither the coarse nor the fine grid simulations fully satisfy Stevens' and Lenschow's (2001) second conjecture regarding use of LES, i.e. that "*the statistics of the low-frequency modes that are explicitly calculated by LES are not sensitive to errors in the parameterization of SGS effects*." Clearly, for the coarse grid, the low frequency (i.e. large spatial scale) features are in fact sensitive to choice of parameterization, not only near the surface, but aloft. The allowable eddy size is increasingly constrained as the solid boundary is approached, while the filter size remains fixed relative to grid spacing (see e. g. Horst et al. 2004), so the fraction of the energy in resolved scales decreases. The models exhibit their greatest differences in these lower layers. Even the finer, 8-m grid produces recognizable differences, although those differences are less pronounced because more energy is in the resolved scales so the requirements of LES are better satisfied.

Differences in w variability, as measured by σ_w, are of great practical importance, because fluctuation intensity directly impacts turbulent fluxes of momentum and scalar variables. That the models produce different standard deviations is interesting, but of itself not particularly enlightening. However, it is noteworthy that the standard deviations shown here do not derive primarily from random spatial distributions, but rather from organized spatial patterns that are recognizably different for different models, not only near the surface, but even well above it. Regardless of resolution or subfilter model, the area encompassed by spatial correlations ≥ 0.2 (Figure 6) spans at least four grid points. At some altitudes, the long axis of a pattern for a given model may extend for more than 20 grid points. This means that the patterns are all well resolved, and that resolved flow solutions depend on both grid spacing and choice of subfilter model.

As might be expected, finer resolution, which leaves less turbulent energy to be modeled, yields smaller differences between the resolved flow structures for different models. However, the increased computational costs that accompany finer resolution may preclude the use of fine grids for many simulations of realistic flows over large (several kilometers or more) areas.

The neutral flow over a flat surface discussed here may be a particularly difficult choice for LES in that there are no major forcing mechanisms driving the resolved flow. It seems reasonable that topography like that found in the geophysical world (see e.g. Chen et al., 2004) will exert forces that may outweigh those from the choice of subfilter model. In such a case, the LES could produce results that closely mimic the forced flow.

There are some reasons to believe that the first Stevens and Lenschow (2001) conjecture ("*The SGS model used in LES is a faithful reproduction of reality*.") might be satisfied by the combined dynamic and near-wall models tested here. Those models produce more realistic mean profiles of wind speed, and smaller, more symmetric, near-surface patterns that seem to be more consistent with observed neutral flows. Away from the wall, eddies are larger and the resolved scales hold a significantly greater fraction of the total energy, so differences among models are less important, but not insignificant (cf., Juneja and Brasseur, 1999). Near the wall, "better" (i. e. dynamic models and the reconstruction models) have a significant impact on the resolved scales. They allow some backscatter of energy, which reproduces the expected interactions of the resolved and subfilter scales (cf., Leslie and Quarini, 1979). The DRM-ADM models mimic this process most faithfully, yielding a much more active spectrum in the smaller scales of the resolved flow. The HATS experiments (Horst et al. 2004) will allow testing and improvement of such models.

Meanwhile, the results presented here show that using LES in lieu of experimental and observational data should be done with considerable caution. The use of LES to examine how surface heat flux and geostrophic wind change the nature of large-scale atmospheric structures served as an example of how such use can be vulnerable to misinterpretation.

Acknowledgments: We gratefully acknowledge the support of National Science Foundation Grants ATM-0453595 [RLS and FLL] and ATM-0645784 [FKC] (Physical Meteorology Program: S. Nelson, Program Director). Acknowledgment is also made to the National Center for Atmospheric Research, which is sponsored by NSF, for computing time used in this research.

References

Andren, A., A. R. Brown, J. Graf, P. J. Mason, C.-H. Moeng, F. T. M. Nieuwstadt, and U, Schumann, 1994: Large-eddy simulation of a neutrally stratified boundary layer: A comparison of four computer codes. *Quart. J. Roy. Meteorol. Soc.,* **120**, 1457-1484.

Bardina, J., J. H. Ferziger, and W. C. Reynolds, 1983: *Improved turbulence models based on large eddy simulation of homogeneous, incompressible, turbulent flows*. Tech. Report TF-19. Dept. of Mech. Eng., Stanford U., Stanford, CA., 174 pp.

Berg, L. K. and S. Zhong, 2005: Sensitivity of MM5-Simulated Boundary Layer Characteristics to Turbulence Parameterization, *J. Appl. Meteorol.,* **44**, 1467–1483.

Bluman, A. G., 2001: *Elementary statistics: a step by step approach, 4th ed*., McGraw-Hill Higher Education, New York, NY, 757 pp.

Brown, A. R., J. M. Hobson and N. Wood, 2001: Large-eddy simulation of neutral turbulent flow over rough sinusoidal ridges. *Bound. Lay. Meteorol.*, **98**, 411-441.

Carati, D., G. S. Winckelmans, and H. Jeanmart, 2001: On the modelling of the subgrid-scale and filtered-scale stress tensors in large-eddy simulation. *J. Fluid Mech.*, **441**, 119-138.

Chen, Q. L. and C. N. Tong, 2006: Investigation of the subgrid-scale stress and its production rate in a convective atmospheric boundary layer using measurement data, *J. Fluid Mech.*, **547**, 65-104.

Chen, Y., F. L. Ludwig, and R. L. Street, 2004: Stably Stratified Flows near a Notched Transverse Ridge across the Salt Lake Valley, *J. Appl. Meteorol.*, **43**, 1308–1328.

Chow, F. K., 2004: *Subfilter-scale turbulence modeling for large-eddy simulation of the atmospheric boundary layer over complex terrain*, PhD dissertation, Dept. of Civil and Environ. Eng., Stanford U., Stanford, CA, 339 pp.

Chow, F. K., R. L. Street, M. Xue and J. H. Ferziger, 2005: Explicit filtering and reconstruction turbulence modeling for large-eddy simulation of neutral boundary layer flow, *J. Atmos. Sci.*, **62**, 2058–2077.

Clark, R. A., J. H. Ferziger, and W. C. Reynolds, 1977: *Evaluation of subgrid-scale turbulence models using a fully simulated turbulent flow*. Tech. Report TF-9. Dept. of Mech. Eng., Stanford U., Stanford, CA., 119 p.

Coleman, G. N., J. H. Ferziger, and P. R. Spalart, 1990: A numerical study of the turbulent Ekman layer, *J. Fluid Mechanics*, **213**, 313-348.

Deardorff, J. W., 1971: On the magnitude of the subgrid scale eddy coefficient., *J. Comp. Phys.,* 7, 120-133.

Dosio, A., J. Vilà-Guerau De Arellano, A. A. M. Holtslag And,P. J. H. Builtjes, 2003: Dispersion of a passive tracer in buoyancy- and shear-driven boundary layers, *J. Appl. Meteorol.*, **42**, 1116-1130.

Dubrulle, B., J.-P. Laval, P. P. Sullivan, and J. Werne, 2002: A New Dynamical Subgrid Model for the Planetary Surface Layer. Part I: The Model and A Priori Tests, *J. Atmos. Sci.*, **59**, 861–876.

Fedorovich, E., 2004: Dispersion of passive tracer in the atmospheric convective boundary layer with wind shears: a review of laboratory and numerical model studies, *Meteorol Atmos Phys.*, **87**, 3–21

Foster, R. C., F. Vianey, P. Drobinski, and P. Carlotti, 2006: Near-surface coherent structures and the vertical momentum flux in a large-eddy simulation of the neutrally-stratified boundary layer, *Boundary-Layer Meteorology*, **120**, 229-255.

Germano, M., U. Piomelli, P. Moin, W. H. and Cabot, 1991: A dynamic subgrid-scale eddy viscosity model, *Phys. of Fluids*, **3**, 1760-1765.

Gullbrand, J. and F. K. Chow, 2003: The effect of numerical errors and turbulence models in large-eddy simulations of channel flow, with and without explicit filtering. *J. Fluid Mech.*, **495**, 323-341.

Hatlee, S. C. and J. C. Wyngaard, 2007: Improved subfilter-scale models from the HATS field data, *J. Atmos. Sci.*, **64**, 1694-.1705.

Horst, T. W., J. Kleissl, D. H. Lenschow, C. Meneveau, C. H. Moeng, M. B. Parlange, P. P. Sullivan and J. C. Weil, 2004: HATS: Field observations to obtain spatially filtered turbulence fields from crosswind arrays of sonic anemometers in the atmospheric surface layer, *J. Atmos. Sci.*, **61**, 1566-1581.

Juneja, A. and J. G. Brasseur, 1999: Characteristics of subgrid-resolved-scale dynamics in anisotropic turbulence, with application to rough-wall boundary layers. *Phys. Fluids*, **11**, 3054-3068.

Khanna, S. and J. G. Brasseur, 1998: Three-dimensional buoyancy- and shear-induced local structure of the atmospheric boundary layer, *J. Atmos. Sci.*, **55**, 710-743.

Kim, S-W, C-H. Moeng, J. C. Weil, and M. C. Barth, 2005: Lagrangian particle dispersion modeling of the fumigation process using large-eddy simulation, *J. Atmos. Sci.*, **62**, 1932-1946.

Kleissl, J., M. B. Parlange and C. Meneveau, 2004: Field experimental study of dynamic Smagorinsky models in the atmospheric surface layer, *J. Atmos. Sci.*, 61, 2296–2307.

Leslie, D. C. and G. L. Quarini, 1979: Application of turbulence theory to the formulation of subgrid modeling procedures, *J. Fluid Mech*, **91**, 65-91.

Lilly, D. K., 1992: A proposed modification of the Germano subgrid-scale closure method, *Phys. of Fluids*, **4**, 633-635.

Lin, C.-L., J. C. McWilliams, C.-H. Moeng, and P. P. Sullivan (1996): Coherent structures and dynamics in a neutrally stratified planetary boundary layer flow, *Physics of Fluids*, **8**, 2626-2639.

Ludwig, F. L., F. K. Chow and R. L. Street, 2006: Effects of sub-filter scale turbulence models on vertical velocity structure in neutral boundary-layer flow, 17th Symp. Bound. Lay. and Turb., (22 -25 May 2006, San Diego , CA), Amer. Meteorol. Soc., paper 4.4

Meneveau, C. and J. Katz, 2000: Scale-invariance and turbulence models for large-eddy simulation, *Annual Rev. Fluid Mech*,, 32, 1–32.

Moeng, C.-H., and J. C. Wyngaard, 1986: An analysis of closures for pressure-scalar covariances in the convective boundary layer. *J. Atmos. Sci.,* 43, 2499–2513.

Nakayama, A., Hori, K., and Street, R. L., 2004: Filtering and LES of flow over irregular rough boundary, *Proc. Summer Program 2004*, Center for Turbulence Research, Stanford U., Stanford, CA, 145-156.

Nakayama, A. and K. Sakio, 2002: Simulation of flows over wavy rough boundaries, *Annual Res. Briefs*, Center for Turbulence Research, NASA Ames and Stanford University, Stanford, CA 313-324.

Nieuwstadt, F. T. M., P. J. Mason, C. H. Moeng, and U. Schumann, 1991: Large-eddy simulation of the convective boundary layer: A comparison of four computer codes. *Selected Papers from the 8th Symposium on Turbulent Shear Flows,* F. Durst, Ed., Springer-Verlag, 343–367.

Porté-Agel,, F., M. Pahlow, C. Meneveau and M. B. Parange, 2001: Atmospheric stability effect on subgrid-scale physics for large-eddy simulation, *Adv. Water Resources*, **24**, 1085-1102.

Smagorinsky, J. 1963 General circulation experiments with the primitive equations. *Mon. Wea. Rev.*, **91**, 99-152.

Sreenivasan, K. R., R. Ramshankar and C. Meneveau, 1989: Mixing, entrainment and fractal dimensions of surfaces in turbulent flows, *Proc. Roy. Soc. London*, **A 421**, 79-108.

Stevens, B, and D. H. Lenschow, 2001: Observations, experiments, and large eddy simulation, *Bull. Amer Meteorol. Soc*, **82**, 283-294.

Stolz, S. and N. A. Adams, 1999: An approximate deconvolution procedure for large-eddy simulation, *Phys. of Fluids*, **11**, 1699-1701.

Takemi, T. and R. Rotunno, 2003: The effects of subgrid model mixing and numerical filtering in simulations of mesoscale cloud systems, *Mon. Wea. Rev.*, **131**, 2085–2101.

van Cittert, P. , 1931: Zum Einflub der Spaltbreite auf die Intensitätsverteilung in Spektrallinien II., *Zeitschrift für Physik*, **69**, 298-308.

Velleman, P. F., 1997: *Data Desk Version 6.0, Handbook 2*, Data Description Inc., Ithaca, NY, 406 pp.

Wong, V. C. and D. K. Lilly, 1994: A comparison of two dynamic subgrid closure methods for turbulent thermal-convection., Phys. of Fluids, 6, 1016-1023.

Woodcock, A. H., 1942: Soaring over the open sea. *Sci. Mon.,* 55, 226-232.

Wyngaard, J. C. , 2004: Toward numerical modeling in the "Terra Incognita," *J. Atmos. Sci.*, **61**, 1816–1826 .

Xue, M., K. K. Droegemeier, and V. Wong, 2000: The Advanced Regional Prediction System (ARPS): A multi-scale nonhydrostatic atmospheric simulation and prediction model. Part I: Model dynamics and verification., *Meteorol. and Atmos. Phys.*, **75**, 161–193.

Xue, M., K. K. Droegemeier, V. Wong, A. Shapiro, and K. Brewster, 1995: *ARPS Version 4.0 User's Guide.*, Center for Analysis and Prediction of Storms, U. of Okla., Norman, OK, 380 pp.

Xue, M., K. K. Droegemeier, V. Wong, A. Shapiro, K. Brewster, F. Carr, D. Weber, Y. Liu, and D. Wang, 2001: The Advanced Regional Prediction System (ARPS): A multi-scale nonhydrostatic atmospheric simulation and prediction tool. Part II: Model physics and applications, Meteorol. and Atmos. Phys., **76**, 143-165.